Fermi surface of LaSb2 and direct observation of a CDW transition

I. Palacio, J. Obando-Guevara, L. Chen, M.N. Nair, M.A. González Barrio, E. Papalazarou, P. Le Fèvre, A. Taleb-Ibrahimi, E.G. Michel, A. Mascaraque, et al.

Fermi surface of $LaSb_2$ and direct observation of a CDW transition

I. Palacio[1,*], J. Obando-Guevara [2,3], L. Chen[2, ¥] , M. N. Nair[1], M.A. González Barrio[3], E. Papalazarou[2], P. Le Fèvre[1], A. Taleb-Ibrahimi[1], E.G. Michel[4], A. Mascaraque[3], A. Tejeda[1,2]

[1] Synchrotron SOLEIL, L'Orme des Merisiers, Saint-Aubin, 91192 Gif sur Yvette, France
[2] LPS, Université Paris Saclay, Orsay, France
[3] Depto Física de Materiales, Universidad Complutense de Madrid, Spain
[4] Depto Física de la Materia Condensada, and Condensed Matter Physics Center (IFIMAC), Universidad Autónoma de Madrid, 28049 Madrid, Spain

¥ Corresponding author

Abstract

We have studied the temperature-dependent electronic structure of the light rare-earth antimonide $LaSb_2$ by combining angle-resolved photoemission (ARPES) measurements and density functional theory (DFT) calculations. ARPES measurements show the appearance of band replicas in the low-temperature Fermi surface with q = 0.25±0.02 A^{-1} and a band folding of the same periodicity with a considerable spectral weight in the folded band. From our calculations we elucidate that the folded band exhibiting the new periodicity is associated with the La-Sb layer. We propose that an in-plane distortion, probably affecting the whole unit cell, is the structural modification related to the electronic changes. All these results converge to support that a charge density wave is stabilized in $LaSb_2$ at low temperature.

Keywords: Layered material, Charge Density Wave, Angle-resolved photoemission, Density Functional Theory

* Now at Instituto de Ciencia de Materiales de Madrid, CSIC, C/ Sor Juana Inés de la Cruz 3, 28049 Madrid, Spain

Charge Density Waves (CDW) have received ample attention and have been actively searched during many years due to their complex and interesting phenomenology [1]. The CDW is a collective state with a periodic symmetry-lowering charge redistribution. The periodicity is determined by the electronic structure, which is modified once the CDW is stabilized, so that the total electronic energy is decreased. The CDW is accompanied by a periodic lattice distortion [2]. It competes sometimes or even coexists with superconductivity in a process not yet well understood [3-8].

The concept of CDW was introduced by Peierls for a one-dimensional metal [2,9]. It requires a periodic lattice distortion of $2k_F$ periodicity (Peierls distortion) and the opening of a band gap at k_F. The Peierls model involves the softening of a phonon related to the periodic lattice distortion, because the one-dimensional response function will peak at $2k_F$, as electrons will screen phonons of this wave vector very efficiently. The one-dimensional Peierls model has been extended to more complex low-dimensional systems using the concept of "nesting", i.e. quasi-1D portions of the Fermi surface that would match after following a rigid displacement in reciprocal space. In this case only partial gapping and nesting would be expected. The experimental phenomenology is complex and the interpretation of the results has been found to be very difficult in many real systems that present a CDW, [10]. For instance, a periodic lattice distortion may appear without apparent changes in the electronic structure [11,12] or the detection of a soft phonon may be elusive [13,14]. In fact, the relevance of Fermi surface nesting to explain charge-ordering transitions has been criticized from different points of view. It has been pointed out that more complex mechanisms that go beyond the Peierls instability have to be invoked in real systems that exhibit a CDW [15], notably the momentum dependence of the electron-phonon interaction [16], i.e. a concerted action of electronic and lattice subsystems [17], and also other phenomena, like excitonic condensation [18] or electron correlations [19]. Extended first-principles calculations have shown that the CDW instabilities may have different physical origins, including the Peierls model [20] but also other mechanisms [21,22].

Layered materials are excellent model systems to investigate these phenomena because they are prone to present CDWs [23,24]. An example of this kind of materials are light rare-earth diantimonides RSb_2 (R=La-Nd). This family of compounds crystallizes in the $SmSb_2$ structure, space group Cmce (64), with alternating layers of Sb and RSb (see Fig. 1) and has a rich and complex physical phenomenology. While $CeSb_2$, $PrSb_2$ and $NdSb_2$ present magnetically ordered states, $LaSb_2$ is non-magnetic. It becomes superconducting at 0.4 K [25] although the onset of the transition is at 2.5 K. The emergence of coherent coupling between layers is believed to be the origin of the observed 2D to bulk transition within the superconducting regime [26].

The magnetoresistance of $LaSb_2$ exhibits a puzzling behavior. It is very large (10 000%) and linear at least up to fields of 45 T [27]. Both its magnitude and its linearity are at odds with the standard semi-classical theory of magnetoresistance [27,28] that predicts a quadratic dependence with magnetic field, except for open Fermi surface orbits, where a saturation for high fields is expected. Several mechanisms may explain a linear magnetoresistance, like local fluctuations in carrier density [29], high field quantization effects [30], disorder or inhomogeneities [31], or magnetic breakdown effects in CDW materials [32]. Carrier density fluctuations and quantization effects are predicted to be measurable only for very low carrier concentrations in extremely high mobility samples, conditions that $LaSb_2$ does not meet. Moreover, the magnetization of $LaSb_2$ displays quantum oscillations [33], and this discards most sources of inhomogeneity and disorder. Finally, linear magnetoresistance has been observed in some materials hosting Dirac fermions [34]. This mechanism has been invoked as the reason for linear magnetoresistance in $LaAgSb_2$, a compound related to $LaSb_2$. In turn, $LaAgSb_2$ is not superconductor, at least down to 0.5 K [35].

A CDW may also be the origin of a linear MR, as observed for the prototypical CDW layered compounds $NbSe_2$ and $TaSe_2$, which display large linear MRs [36]. A CDW could be present in $LaSb_2$, as energy band structure calculations [33] predict significant nesting between the Fermi surface sheets that produce experimental open orbits, which cannot be detected in de Haas-van Alphen experiments [33]. Furthermore, related compounds like $LaAgSb_2$ [37] or $La_{1-x}Ce_xSb_2$ [38] exhibit CDW ordering. Due to these reasons, a CDW in $LaSb_2$ has been actively searched. The kink in the resistivity found for $La_{1-x}Ce_xSb_2$ in a broad range of Ce concentrations was considered the evidence of a CDW in this solid solution [38]. The observation of a correlated kink in $LaSb_2$ at 355 K would point to the formation of a CDW in this material as well [36]. However, STM experiments did not find clear evidence of a CDW phase at 0.15 K [39]. Thus, neither previous photoemission experiments at 140 K [40] nor STM experiments at 0.15 K [39] have found indications of CDW formation. Finally, Fisher and coworkers [41] have proposed that defects in the crystalline structure (twinning or stacking faults) could be behind the CDW state and the unsaturating linear magnetoresistance.

In this work, we report a temperature-driven phase transition that modifies the Fermi surface and the band structure, leading to the appearance of band replicas at low temperature associated with a reciprocal lattice vector q related to k_F. Density functional theory (DFT) calculations on distorted and undistorted structures allow to interpret and understand the experimental results and explain them by the stabilization of a CDW.

Experimental and calculation details

$LaSb_2$ single crystals are grown from high purity La and Sb by the metallic flux method [42]. The experiments are carried out in an ultrahigh vacuum (UHV) chamber with a base pressure below 10^{-10} mbar. Angle-resolved photoelectron spectroscopy (ARPES) is performed using a Scienta R4000 electron analyzer (±15° acceptance angle) at the Cassiopeé beamline of SOLEIL synchrotron radiation laboratory. The base energy resolution is better than 1 meV with 0.1° angular resolution. ARPES experiments are performed after in-situ cleaving the samples under ultrahigh-vacuum conditions. The sample cleaves between the La/Sb bilayer, exposing a surface that it is composed by (001) Sb atomic planes. The quality of the cleavage is good in regions much wider than the photon beam.

Density Functional Theory (DFT) electronic band calculations are carried out [43] by combining the Vienna ab-initio simulation package (VASP) [44,45] and post-processing with the VASPKIT package [46]. The Generalized Gradient Approximation (GGA) in the Perdew, Burke, Ernzerhof (PBE) formulation [47] is used for the exchange-correlation potential. The cutoff energy is set to 500 eV. A Monkhorst-Pack [48,49] k-meshes with a size of 8×8×2 for the $LaSb_2$ primitive cell and a size of 8×2×2 for the $LaSb_2$ supercell are used for the geometry optimization. The self-consistent field convergence for the total energy and the force variation are set to 10^{-6} eV and 0.001 eV/Å, respectively.

Results and discussion

Fig.1a shows the crystalline structure of $LaSb_2$ (a=b=4.483 Å, c= 18.671 Å). The structure presents alternating Sb 2D sheets and La/Sb bilayers, so that Sb 2D sheets are sandwiched between the corrugated La/Sb bilayers along the c axis. Fig. 1a shows the primitive cell, together with a conventional unit cell, more convenient for visualizing the structure. The corners of the square basis of the primitive cell are located in the middle points of the sides of the square basis of the conventional cell on the (001) surface. Fig.1b shows the Brillouin zone of the $LaSb_2$ primitive cell and the k_x, k_y, k_z axis corresponding to the a, b, c axis in real space in Fig.1a, respectively.

We have calculated the electronic structure of $LaSb_2$ and the results are shown in Figs. 1c-g. Fig.1c presents the 3D Fermi surface. The Fermi surface consists of two main pieces: a large diamond (warped square) and two glasses-like pockets. Unlike other compounds of the same family, like $LaAgSb_2$ [50], in $LaSb_2$ there are no Fermi surface sheets centered on the $\bar{\Gamma}$ point [51]. The two glasses-like pockets run along the $\bar{\Gamma}\rightarrow\bar{Y}$ direction and each of them contains two sheets (yellow and green in Fig. 1c). The warped square contains also two sheets (blue and red in Fig. 1c) that extend to the edges of the Brillouin zone, with corners that are located at $\bar{S}$ points. Four additional small pockets (purple in Fig. 1c) are located at the $\bar{S}$ points. The Fermi surface sheets found are in agreement

with previous calculations and with results from de Haas-van Alphen experiments [33,52]. Furthermore, based on the Fermi surface image, we can observe that the dispersion along k_z is small, in agreement with the quasi two-dimensional nature of the electronic structure of a layered material.

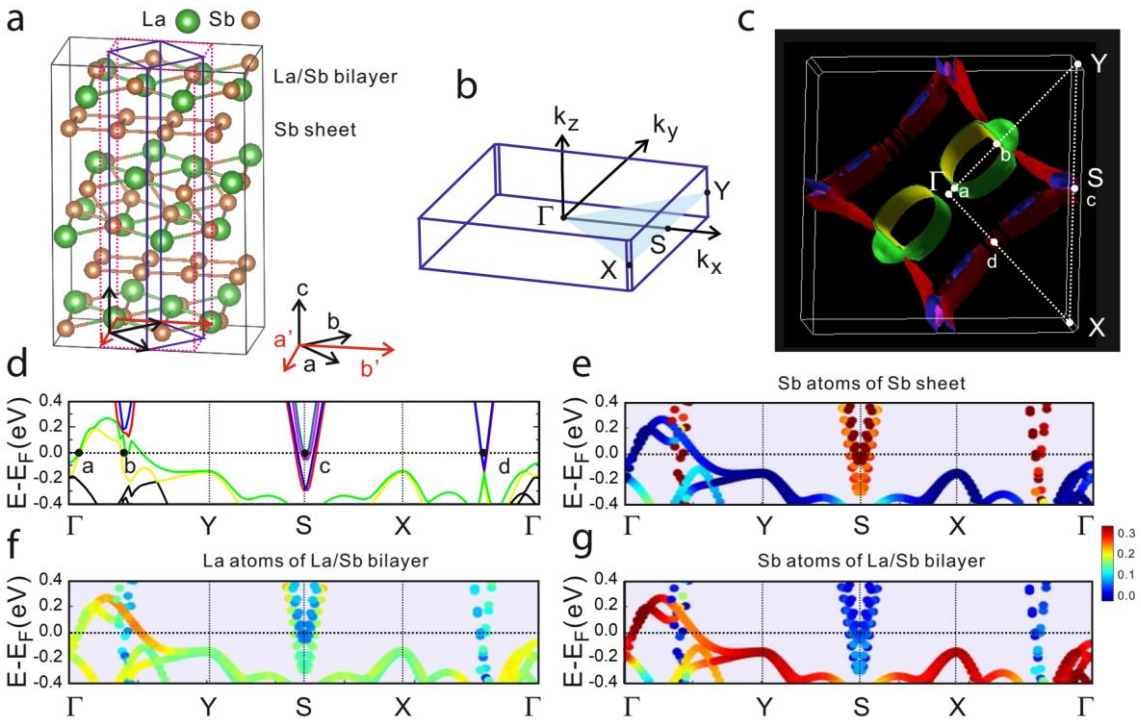

Fig. 1 (a). Layered $LaSb_2$ crystalline structure, formed by Sb sheets and La/Sb bilayers. The primitive and conventional cells are marked with blue and red lines, respectively. b. Brillouin zone corresponding to the $LaSb_2$ primitive cell. (c-g) Theoretical electronic band structure of $LaSb_2$ c. Calculated Fermi surface of $LaSb_2$. The Fermi surface sheets are highlighted using different colors: yellow and green for the inner glasses-like pockets, blue and red for the outer warped square and purple for the small pockets near $\bar{S}$ points. d-h. Electronic band structures of $LaSb_2$ along Γ-Y-S-X-Γ K paths. The band structure is projected on the Sb atoms of the Sb-sheets (e), La atoms of the La/Sb bilayers (f), and Sb atoms of the La/Sb bilayers (g). The color scale indicates the contribution for each band at the different atoms (red is higher). The crossing points of the bands with the Fermi energy (a,b,c,d) are roughly marked in panels c and d.

The electronic band structure along Γ-Y-S-X-Γ K paths is shown in Fig.1d-g. The energy range of the calculated band structure is restricted to values around the Fermi energy in order to compare the calculations with experimental bands more clearly (see below). Fig.1d shows the bands crossing the Fermi level (crossing points marked by a,b,c,d). In order to better relate the band structure and the Fermi surface, these crossing points are also indicated in the Fermi surface shown in Fig.1c. Further information on the Fermi surface sheets is extracted from the atomic origin of the bands. Figs. 1e-g show the atom-projected band structures. Fig. 1e corresponds to projection on the Sb atoms of the Sb-

sheets, Fig. 1f on the La atoms of the La/Sb bilayers, and Fig. 1g on the Sb atoms of the La/Sb bilayers. Note that the warped square sheets of the Fermi surface have a strong Sb content from atoms in the Sb sheets (Fig. 1e). These bands present quasi-conical dispersion near the $\bar{S}$ points (Fig. 1e). The two glasses-like pockets in the Fermi surface arise mainly from the La and Sb atoms in the La/Sb bilayers, as shown in Figs. 1f and 1g. A close inspection of the Fermi surface shown in Fig. 1c reveals sheets that are parallel to each other, susceptible to nest and therefore favorable to induce a CDW instability, as previously suggested [33]. Nesting implies that significant parts of the Fermi surface are connected by a wave vector q [9]. In this case, replicas of the Fermi surface sheets appear when the CDW sets in [53,54]. In the search for changes in the electronic structure of $LaSb_2$ related to a CDW, which have been elusive up to now, we have performed ARPES measurements covering an extended area of reciprocal space. The intensity at the Fermi level is obtained by integrating the spectral weight in a window of ±20 meV around the Fermi energy. Fig. 2a, b show the Fermi surface of $LaSb_2$ at T=200 K and T=13 K respectively (a larger region of the reciprocal space is shown in the Supplementary Material) for $h\nu$= 118 eV. At 200 K the shape of the experimental Fermi surface reproduces the warped square and the glasses-like pockets. When the temperature is lowered to T=13 K, the shape of the Fermi surface changes dramatically. As seen Fig. 2b, the Fermi surface is replicated along the $\overline{\Gamma Y}$ direction, the same direction along which the glasses-like pockets are oriented. In order to analyze these changes in detail, we have made several cuts in the Fermi surface parallel to this direction. The cuts have been made both perpendicular to the outer edge of the warped square (yellow arrows in Fig. 2a, b) and along the glasses-like portions (Fig. S1). These cuts (labelled with numbers) are represented in Fig. 2c, d. The maxima of the intensity are highlighted with colored dots and the location of the maxima in reciprocal space is shown in Fig. 2a, b. While at T=200 K only one maximum appears, at T=13 K a replica is observed. The separation between the two maxima is constant and corresponds to a value of q= 0.25 ± 0.02 A^{-1} (equivalent to (0.18 ± 0.01) $2\pi/a$). The Supplementary material shows additional analysis of Fermi surface regions interconnected by this q vector.

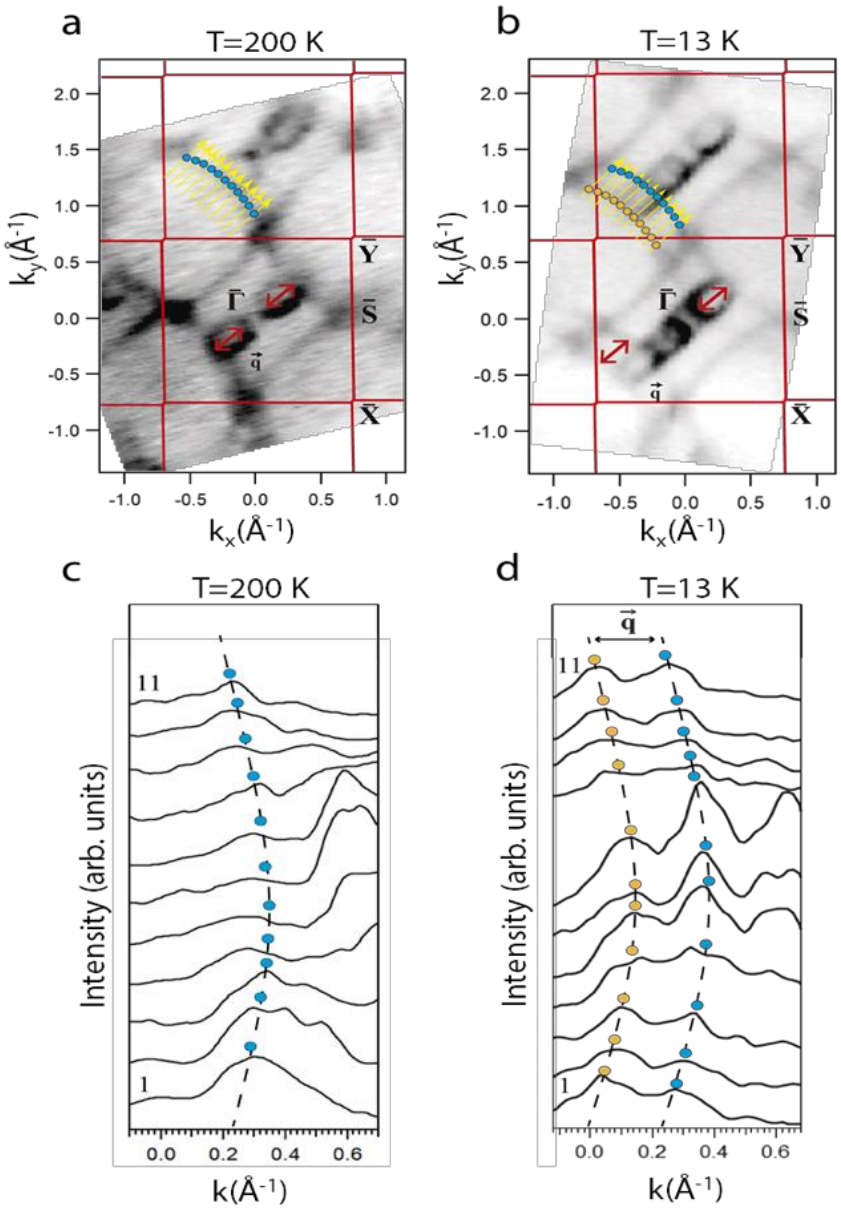

Fig. 2. Experimental k-space mapping of the Fermi surface obtained from the plot of the ARPES intensity as a function of the k_x and k_y vectors near the Fermi level ($h\nu$= 118 eV). The measurements are done at (a) T=200 K and (b) T=13 K. The panels cover the first and second Brillouin zones. Yellow arrows indicate the places where cuts of the Fermi surface are done. The cuts corresponding to the second Brillouin zone, labeled by numbers, are represented in panels (c) and (d) respectively, where k=0 corresponds to the arrow start. The blue and yellow dots in these panels indicate the intensity maxima. While at high temperature there is only one maximum, i.e., one band crossing the FL (blue dots), at low temperature there are two bands (yellow dots). The maxima are separated by a distance q= 0.25 ± 0.02 A^{-1}. This vector (length and direction) is depicted in panel (b).

We present the electronic structure measured by ARPES along the high symmetry directions of the Brillouin Zone ($\bar{\Gamma}\bar{Y}\bar{S}\bar{X}\bar{\Gamma}$) in Fig. 3, measured at 200 K and at 13 K. After cleaved, the exposed surface is composed by (001) Sb atomic planes (Fig. 1a). Fig. 3 represents the curvature plot [55] of the ARPES intensity obtained with a photon energy of hν=118 eV on a wide range of binding energy. The curvature analysis is a powerful method to enhance dispersive features in a spectroscopic image and is typically used to highlight the region near the Fermi level, whose intensity may be weak in comparison with the rest of the band structure. There are clear modifications as a function of the temperature in the high binding energy bands. At high temperature, there are two low-dispersing bands around -0.5 eV and -1.0 eV, whose energy difference increases at low temperature. The observed changes in binding energy and dispersion might be attributed to band Umklapps and/or to increased correlation effects in the low temperature phase, but further work is needed to discriminate the origin. However, the most important difference between the data at 200 K and at 13 K is seen in the Fermi level region, where electronic instabilities are relevant. In the neighborhood of $\bar{\Gamma}$ along the $\overline{\Gamma Y}$ direction, the bands present a strong folding at 13 K. This modification of the band structure corresponds to the glasses-like pockets associated with the La-Sb bands (red rectangle in Fig. 3a, b). This region is enlarged in Fig. 3c, d, which shows how these bands are folded at low temperature. The spectral weight in the folded band is very strong, indicating that a strong potential is inducing the folding. Simultaneously to the band folding, it seems to be a weight reduction in the lowest binding energy states at low temperature. A spectral weight reduction in the whole Brillouin zone is compatible with Mott transitions, that can be triggered by the bandwidth reduction W due to CDW band folding, since the W/U ratio (U being the electronic correlation) is more favorable for Mott physics [12]. Figure 3 does not exhibit gap opening. The intensity decreases at the Fermi energy associated to the band gap of the CDW can only be observed when the CDW gap is larger than the width of the bands. Not observing the band gapping at the Fermi surface only means that the band gap is possibly smaller than the width of the electronic bands (here around 100 meV). Since the transition temperature is somewhere between 200 K and 13 K, the maximum band gap could be associated to 200 K, i.e., 18 meV. Therefore, in this case the intrinsic width of the electronic bands does not allow us to observe the band gap at the Fermi surface.

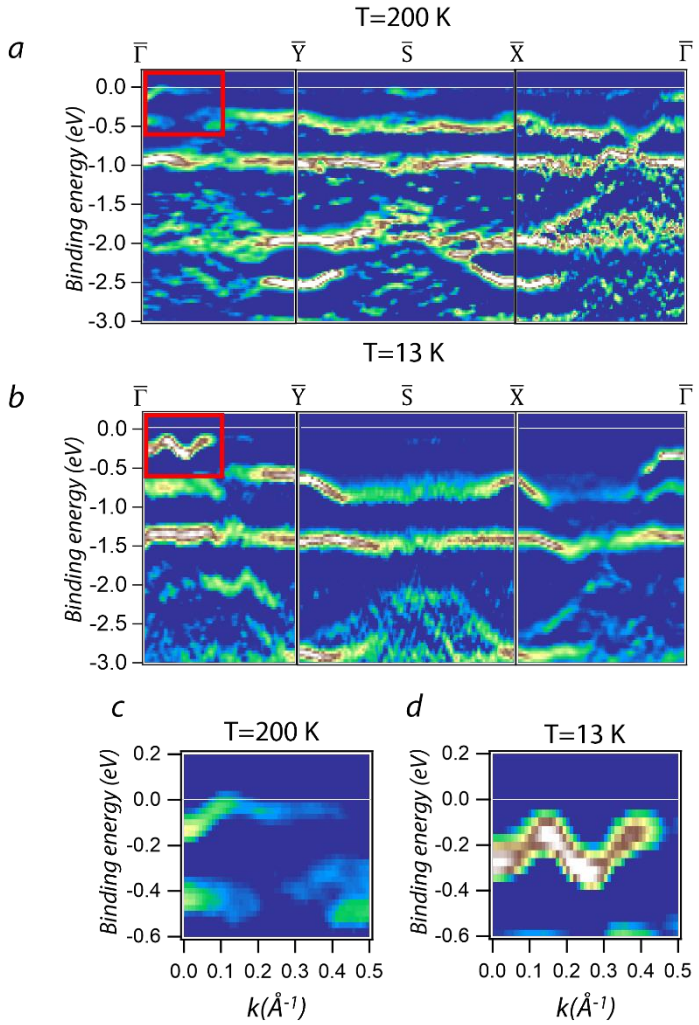

Fig. 3 Experimental band structure along high symmetry directions ($\bar{\Gamma}\bar{Y}\bar{S}\bar{X}\bar{\Gamma}$) at (a) 200 K and (b) 13 K. Panels (c) and (d) are zooms of the areas indicated with a red rectangle in panels (a) and (b) respectively.

The experimental results at low temperature show both replicas at the Fermi surface and a clear folding of a La-Sb band. Replicas are connected to the original spectral features by a reciprocal space vector of the size of the La-Sb pocket. This corresponds to one-third of the $\overline{\Gamma Y}$ distance, so that the periodicity of the atomic structure in real space should be 3 times larger along the **b'** direction (i.e., 3**b'**, see Fig. 1a). These electronic changes are compatible with the stabilization of a CDW at low temperature (13 K). The data at 200 K reflect the electronic structure of the high temperature phase (normal phase). In order to understand the nature of the structural distortion associated with this wave vector, we have constructed a supercell of size 3**b'**, i.e. it contains 3 conventional cells along the **b'** direction, since this size will allow us to describe the observed q vector. Fig. 4a shows a supercell with no structural modification (called hereafter *pristine* supercell) and corresponding to the high-temperature phase. In order to

obtain an effective primitive cell band structure, unfolded band structures [56] are calculated for the supercells studied. Fig.4b shows the unfolded band structure of the pristine supercell, where we observe that the bands are in reasonable agreement with the bands of the primitive cell (Fig.1).

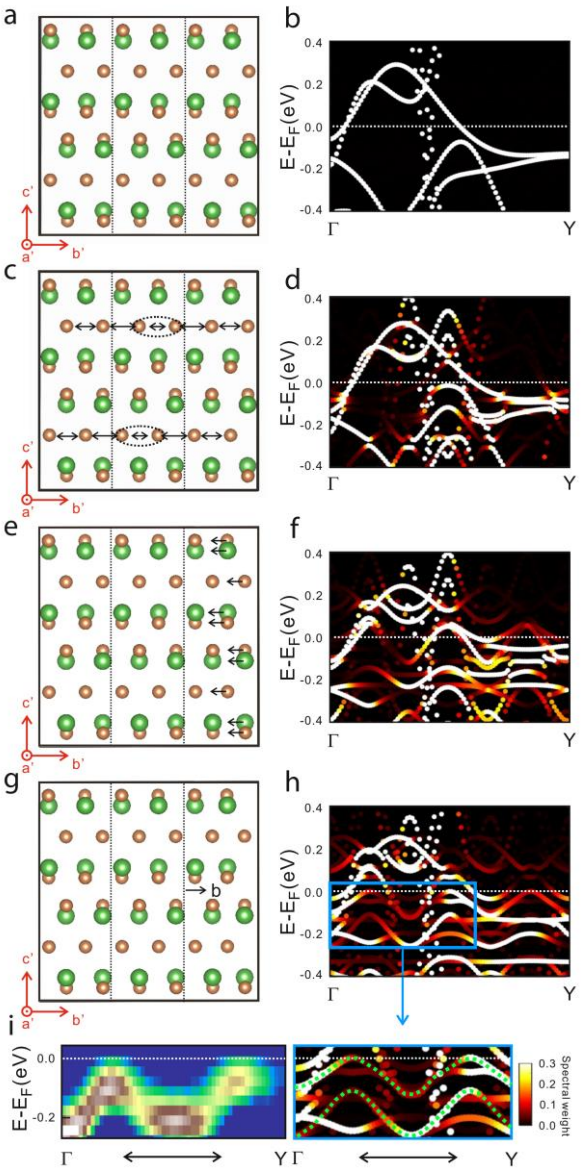

Fig. 4. Structural modifications and the corresponding band structures. (a) Supercell of $LaSb_2$ containing 3 conventional cells along **b'** direction. (b) Unfolded band structure of the supercell in (a). (c), (e), (g). $LaSb_2$ supercells with modified atomic positions to simulate the periodicity of the CDW: (c) Displacement of the Sb atoms in Sb sheets along **b'** direction to introduce a longitudinal-wave-like modification in the Sb sheet. (e) Displacement of half of the atoms in the conventional unit cell (those in the right conventional cell). (g) Displacement of the whole middle conventional cell by 0.02 Å along the **b'** direction. (d), (f), (h). Unfolded band structures correspond to the modified supercells in (c), (e), and (g), respectively. (i) Area near E_F from the experimental band structure (Fig. 3b)

and theoretical band structure of an atomic distortion affecting the whole unit cell (h).

Considering that this supercell describes the electronic structure at 200 K (high-temperature phase), we focus on describing the low-temperature phase. The experimental results show a clear folding of the glass-like features, corresponding to one-third of the $\overline{\Gamma}$-$\overline{Y}$ distance, i.e. 3**b'** in real space or equivalently 3 times along the **a**+**b** direction. This information is hard to obtain straightforwardly from DFT. As DFT calculations are static simulations, temperature-dependent changes are difficult to simulate [57]. Therefore, in order to calculate the low-temperature crystal structure, we have forced different structural modifications in the pristine supercell. The displacements correspond to the experimental q vector of the CDW. This procedure induces a CDW in the system corresponding to the experimental **q** vector. We have analyzed several structural modifications with a **3b**' periodicity. In particular, we have introduced displacements (1) on the Sb sheets, (2) on part or (3) on all of the atoms of one conventional cell. Fig.4c shows a longitudinal-wave-like modification in the Sb sheets (method 1), where Sb atoms in Sb sheets are displaced along **b'** direction. The two middle Sb atoms in the Sb sheets are displaced towards each other along **b'** direction, reducing their distance by 0.03 Å. Then we fix these atoms, and the positions of the rest of the atoms are relaxed. Fig. 4e shows the displacement of half of the atoms in the conventional unit cell. Atoms on the right side of the unit cell are shifted by 0.02 Å along **b'** direction. Then, the right-part of the conventional cell is fixed and again all the other atoms are relaxed (method 2). Fig. 4g shows the displacement of the whole middle conventional cell along **b'** direction by 0.02 Å (method 3). This represents a wave like distortion along **b'**. Furthermore, we have also tried many other structural modifications, such as displacement of the Sb atoms in Sb sheets by 0.03 Å along **a'** direction, displacement of the Sb atoms inside the right-side conventional cell 0.02 Å and 0.04 Å along **b'** direction, and displacement of the whole middle conventional cell by 0.02 Å along the **a'** direction and **c'** direction, which are shown in the Supplementary Material. The unfolded band structures of these different modified structures are shown in Fig.4 and Fig.S4.

We want to stress that not every structural modification of the periodicity reproduces the experimental band structure. We also observe that the distorted structures introduce more bands, compared to the unfolded band structure of the pristine supercell. Band replicas are observed for some structural deformations, such as Fig.4d,h and Fig.S4d,f,j. In particular, the displacement of the whole conventional middle cell along **b'** direction (method 3)) shows more clearly band replicas and also the band shapes are almost preserved (Fig.4h). A detailed comparison of the experimental and calculated band structures with this structural distortion are shown together for comparison in Fig.4i. There is a fair

agreement with the experiment. Note the presence of band replicas just below the Fermi level with a dispersion similar to the experimental bands. This rough model captures the essential physics of the system, so the temperature-driven phase transition of $LaSb_2$ is traced back to a periodic distortion of the structure along the **b'** direction, involving most of the atoms of the conventional unit cell. The atomic displacements introduced are in the range of 0.02-0.03 Å. For much smaller displacements, band replicas are hard to observe, and for much higher displacements, the band structure deviates seriously from the original one (see for instance Fig.S4f). Since the experimental low temperature bands and Fermi surface keep the original shape, except for the replicas, the structural modifications cannot deviate much from the above-mentioned values. We conclude that the displacements that originate de CDW are roughly in the range of 0.02-0.03 Å.

It is interesting to compare the periodicity of the CDW observed at low temperature with the periodicities identified previously for the related compound $LaAgSb_2$. We would like to point out that this comparison should be made with care, because the two compounds have a closely related structure and composition, although the shape of their Fermi surfaces is different, in particular the number and shape of the Fermi surface sheets are not the same. The CDW of $LaAgSb_2$ presents a periodic lattice distortion with a periodicity corresponding to 0.026 $2\pi/a$ [37], much smaller than the value of 0.18 $2\pi/a$ found in this work for $LaSb_2$. In turn, the small value found for $LaAgSb_2$ hinders the observation of modifications in the electronic structure. In fact, the effects related to the stabilization of the CDW are limited to a reduction of intensity in the region close to the Fermi energy [58]. An analysis of the region close to the Fermi energy in $LaSb_2$ shows the strong band folding observed in Figs. 3c,d. It is interesting to analyze the behavior in the rest of the reciprocal space as well. The observation of folding in Fig. 3c,d does not involve gapping, as shown by the theoretical folding depicted in Fig. 4i and evidenced by the observation of replicas in the Fermi Surface in Fig. 2b. We note that the less intense bands near the Fermi level area are hardly seen in the curvature plot of Fig. 3b. If we want to compare the intensity of the bands near the Fermi energy for the high temperature phase (200 K) and the CDW phase (13 K), we need to resort to the original data, as the curvature plot may induce a relative change of intensity of the bands. This analysis is made in the Supplementary Information, where Fig. S2 and S3 show an intensity reduction near the Fermi energy, without any apparent gapping, as observed for $LaAgSb_2$, and in agreement with de Haas-van Alphen measurements [33], which did not find Fermi surface sections affected by a possible CDW at low temperature.

Finally, it is worth to compare these findings with the results for $La_{1-x}Ce_xSb_2$ [38] as well. The substitution of La by Ce generates a pronounced kink in the resistivity vs. temperature, also observed in the specific heat, suggestive of the

formation of a CDW. An analogous kink in the resistivity for $LaSb_2$ would correspond to a CDW in this material at 355 K, i.e. well above the temperature range found in this work. However, sequential CDW distortions are not rare, as they have been observed in several compounds, like the very closely related compound LaAgSb2 (207 K and 16 K), and in other compounds such as 2H-TaSe2 (122 K and 90 K), 1T-TaS2 (1120 K, 350 K, 180 K), NbSe3 (145 K, 59 K) [12,32,37,59-61]. As no specific periodic lattice distortion was reported for $La_{1-x}Ce_xSb_2$, it is not possible to establish any relationship between the CDW at 355 K and the CDW found here below 200 K and experimentally observed at 13 K, although sequential CDW distortions have been observed in several compounds [12,32,37,59-61].

In summary, ARPES measurements reveal the presence of changes in the electronic structure of $LaSb_2$ surface between 200 K and 13 K, including band folding and replicas in the Fermi surface. All these modifications are signatures of the stabilization of a CDW appearing below 200 K and observed at 13 K, above the superconducting critical temperature of the system (0.4 K). The changes in the electronic structure at low temperature are related to the same q vector ($q = 0.25\pm0.02$ Å^{-1}), indicating that they correspond to an intrinsic property of the CDW phase. The q vector found connects regions inside the glasses-like pockets of the Fermi surface. The results of theoretical calculations permit to interpret these findings. The calculations show that the glasses-like pockets involved in the CDW transition exhibit La-Sb character and that the transition corresponds to a small structural distortion affecting all the atoms in the unit cell. We also propose that the CDW transition appearing at 13 K could trigger a Mott transition at lower temperatures due to the bandwidth reduction, as in other systems, a scenario worth exploring.

ACKNOWLEDGEMENTS

This work was supported by the French Agence Nationale de la Recherche (ANR) contracts ref. NT-09-618999. MAG and AM thank Ministerio de Ciencia e Innovación (project PID2020-117024GB-C43) and Comunidad de Madrid (project S2108–NMT4321) for financial support. EGM thanks Ministerio de Ciencia e Innovación (project PCI2022-132998) and the “María de Maeztu” Programme for Units of Excellence in R&D (CEX2018-000805-M). We also thank all CASSIOPEE staff from synchrotron SOLEIL for support during ARPES beam times, D. Malterre, Vincent Jacques, David le Bolloc’h, H. Suderow and P.C.

Canfield for helpful discussions. We thank H. Suderow and P.C. Canfield for providing the $LaSb_2$ samples.

References

[1] C. Schlenker, J. Dumas, M. Greenblatt, S. van Smaalen, eds., Physics and Chemistry of Low-Dimensional Inorganic Conductors, Springer US, Boston, MA, 1996.

[2] M.J. Rice, S. Strässler, Effects of fluctuations and interchain coupling on the peierls transition, Solid State Commun. 13 (1973) 1389–1392.

[3] H.M. Hill, S. Chowdhury, J.R. Simpson, A.F. Rigosi, D.B. Newell, H. Berger, F. Tavazza, A.R.H. Walker, Phonon origin and lattice evolution in charge density wave states, Phys. Rev. B. 99 (2019) 174110.

[4] F.H. Yu, D.H. Ma, W.Z. Zhuo, S.Q. Liu, X.K. Wen, B. Lei, J.J. Ying, X.H. Chen, Unusual competition of superconductivity and charge-density-wave state in a compressed topological kagome metal, Nat. Commun. 12 (2021) 3645.

[5] Y. Song, T. Ying, X. Chen, X. Han, X. Wu, A.P. Schnyder, Y. Huang, J. Guo, X. Chen, Competition of Superconductivity and Charge Density Wave in Selective Oxidized CsV_3Sb_5 Thin Flakes, Phys. Rev. Lett. 127 (2021) 237001.

[6] J. Chang, E. Blackburn, A.T. Holmes, N.B. Christensen, J. Larsen, J. Mesot, R. Liang, D.A. Bonn, W.N. Hardy, A. Watenphul, M. v Zimmermann, E.M. Forgan, S.M. Hayden, Direct observation of competition between superconductivity and charge density wave order in $YBa_2Cu_3O_{6.67,}$ Nat. Phys. 8 (2012) 871–876.

[7] A.H. Castro Neto, Charge Density Wave, Superconductivity, and Anomalous Metallic Behavior in 2D Transition Metal Dichalcogenides, Phys. Rev. Lett. 86 (2001) 4382–4385.

[8] T.P. Croft, C. Lester, M.S. Senn, A. Bombardi, S.M. Hayden, Charge density wave fluctuations in $La_{2-x}Sr_xCuO_4$ and their competition with superconductivity, Phys. Rev. B. 89 (2014) 224513.

[9] R.E. Peierls, R.S. Peierls, Quantum theory of solids, Oxford University Press, 1955.

[10] X. Zhu, J. Guo, J. Zhang, E.W. Plummer, Misconceptions associated with the origin of charge density waves, Adv. Phys. X. 2 (2017) 622–640.

[11] X. Zhu, W. Ning, L. Li, L. Ling, R. Zhang, J. Zhang, K. Wang, Y. Liu, L. Pi, Y. Ma, H. Du, M. Tian, Y. Sun, C. Petrovic, Y. Zhang, Superconductivity and Charge Density Wave in $ZrTe_{3-x}Se_x$, Sci. Rep. 6 (2016) 26974.

[12] M. Bovet, D. Popović, F. Clerc, C. Koitzsch, U. Probst, E. Bucher, H. Berger, D. Naumović, P. Aebi, Pseudogapped Fermi surfaces of 1T-TaS_2 and 1T-$TaSe_2$ A charge density wave effect, Phys. Rev. B. 69 (2004) 125117.

[13] R. Pérez, J. Ortega, F. Flores, Surface Soft Phonon and the $\sqrt{3}x\sqrt{3} \leftrightarrow 3x3$ Phase Transition in Sn/Ge(111) and Sn/Si(111), Phys. Rev. Lett. 86 (2001) 4891–4894.

[14] D. Farías, W. Kamiński, J. Lobo, J. Ortega, E. Hulpke, R. Pérez, F. Flores, E.G. Michel, Phonon Softening, Chaotic Motion, and Order-Disorder Transition in Sn/Ge(111), Phys. Rev. Lett. 91 (2003) 016103.

[15] M.D. Johannes, I.I. Mazin, C.A. Howells, Fermi-surface nesting and the origin of the charge-density wave in $NbSe_2$, Phys. Rev. B. 73 (2006) 205102.

[16] M. Calandra, I.I. Mazin, F. Mauri, Effect of dimensionality on the charge-density wave in few-layer 2H-$NbSe_2$, Phys. Rev. B. 80 (2009) 241108.

[17] M.D. Johannes, I.I. Mazin, Fermi surface nesting and the origin of charge density waves in metals, Phys. Rev. B. 77 (2008) 165135.

[18] C. Monney, E.F. Schwier, M.G. Garnier, N. Mariotti, C. Didiot, H. Cercellier, J. Marcus, H. Berger, A.N. Titov, H. Beck, Probing the exciton condensate phase in 1T-TiSe2 with photoemission, New J. Phys. 12 (2010) 125019.

[19] J.C. Petersen, S. Kaiser, N. Dean, A. Simoncig, H.Y. Liu, A.L. Cavalieri, C. Cacho, I.C.E. Turcu, E. Springate, F. Frassetto, L. Poletto, S.S. Dhesi, H. Berger, A. Cavalleri, Clocking the Melting Transition of Charge and Lattice Order in 1T-TaS_2 with Ultrafast Extreme-Ultraviolet Angle-Resolved Photoemission Spectroscopy, Phys. Rev. Lett. 107 (2011) 177402.
[20] B. Guster, M. Pruneda, P. Ordejón, E. Canadell, J.-P. Pouget, Evidence for the weak coupling scenario of the Peierls transition in the blue bronze, Phys. Rev. Mater. 3 (2019) 055001.
[21] B. Guster, E. Canadell, M. Pruneda, P. Ordejón, First principles analysis of the CDW instability of single-layer 1T-$TiSe_2$ and its evolution with charge carrier density, 2D Mater. 5 (2018) 025024.
[22] B. Guster, R. Robles, M. Pruneda, E. Canadell, P. Ordejón, 2 × 2 charge density wave in single-layer $TiTe_2$, 2D Mater. 6 (2018) 015027.
[23] E. Piatti, Q. Chen, M. Tortello, J. Ye, R.S. Gonnelli, Possible charge-density-wave signatures in the anomalous resistivity of Li-intercalated multilayer MoS_2, Appl. Surf. Sci. 461 (2018) 269–275.
[24] A. Ghafari, L. Petaccia, C. Janowitz, Splitting of the Ti-3d bands of $TiSe_2$ in the charge-density wave phase, Appl. Surf. Sci. 396 (2017) 1649–1656.
[25] F. Hulliger, H.R. Ott, Superconductivity of lanthanum pnictides, J. Common Met. 55 (1977) 103–113.
[26] S. Guo, D.P. Young, P.W. Adams, X.S. Wu, J.Y. Chan, G.T. McCandless, J.F. DiTusa, Dimensional crossover in the electrical and magnetic properties of the layered $LaSb_2$ superconductor under pressure: The role of phase fluctuations, Phys. Rev. B. 83 (2011) 174520.
[27] D.P. Young, R.G. Goodrich, J.F. DiTusa, S. Guo, P.W. Adams, J.Y. Chan, D. Hall, High magnetic field sensor using $LaSb_2$, Appl. Phys. Lett. 82 (2003) 3713–3715.
[28] N.W. Ashcroft, N.D. Mermin, Solid state physics, (1976).
[29] S.H. Simon, B.I. Halperin, Explanation for the Resistivity Law in Quantum Hall Systems, Phys. Rev. Lett. 73 (1994) 3278–3281.
[30] A.A. Abrikosov, Quantum linear magnetoresistance, EPL Europhys. Lett. 49 (2000) 789.
[31] M.M. Parish, P.B. Littlewood, Non-saturating magnetoresistance in heavily disordered semiconductors, Nature. 426 (2003) 162–165.
[32] J.A. Wilson, F.J. Di Salvo, S. Mahajan, Charge-density waves and superlattices in the metallic layered transition metal dichalcogenides, Adv. Phys. 24 (1975) 117–201.
[33] R.G. Goodrich, D. Browne, R. Kurtz, D.P. Young, J.F. DiTusa, P.W. Adams, D. Hall, de Haas--van Alphen measurements of the electronic structure of $LaSb_2$, Phys. Rev. B. 69 (2004) 125114.
[34] K. Wang, D. Graf, H. Lei, S.W. Tozer, C. Petrovic, Quantum transport of two-dimensional Dirac fermions in $SrMnBi_2$, Phys. Rev. B. 84 (2011) 220401.
[35] Y. Muro, N. Takeda, M. Ishikawa, Magnetic and transport properties of dense Kondo systems, $CeTSb_2$(T=Ni, Cu, Pd and Ag), J. Alloys Compd. 257 (1997) 23–29.
[36] M. Naito, S. Tanaka, Galvanomagnetic Effects in the Charge-Density-Wave State of 2H-$NbSe_2$ and 2H-$TaSe_2$, J. Phys. Soc. Jpn. 51 (1982) 228–236.
[37] C. Song, J. Park, J. Koo, K.-B. Lee, J.Y. Rhee, S.L. Bud'ko, P.C. Canfield, B.N. Harmon, A.I. Goldman, Charge-density-wave orderings in $LaAgSb_2$ An x-ray scattering study, Phys. Rev. B. 68 (2003) 035113.
[38] R.F. Luccas, A. Fente, J. Hanko, A. Correa-Orellana, E. Herrera, E. Climent-Pascual, J. Azpeitia, T. Pérez-Castañeda, M.R. Osorio, E. Salas-Colera, N.M. Nemes, F.J. Mompean, M. García-Hernández, J.G. Rodrigo, M.A. Ramos, I. Guillamón, S. Vieira, H. Suderow, Charge density wave in layered $La_{1-x}Ce_xSb_2$, Phys. Rev. B. 92 (2015) 235153.
[39] J.A. Galvis, H. Suderow, S. Vieira, S.L. Bud'ko, P.C. Canfield, Scanning tunneling microscopy in the superconductor $LaSb_2$, Phys. Rev. B. 87 (2013) 214504.

[40] A.I. Acatrinei, D. Browne, Y.B. Losovyj, D.P. Young, M. Moldovan, J.Y. Chan, P.T. Sprunger, R.L. Kurtz, Angle-resolved photoemission study and first-principles calculation of the electronic structure of $LaSb_2$, J. Phys. Condens. Matter. 15 (2003) L511.
[41] K.F. Fischer, N. Roth, B.B. Iversen, Transport properties and crystal structure of layered LaSb2, J. Appl. Phys. 125 (2019) 045110.
[42] P.C. Canfield, J.D. Thompson, Z. Fisk, Novel Ce magnetism in CeDipnictide and Di-Ce pnictide structures, J. Appl. Phys. 70 (1991) 5992–5994.
[43] W. Kohn, L.J. Sham, Self-consistent equations including exchange and correlation effects, Phys. Rev. 140 (1965) A1133.
[44] G. Kresse, J. Furthmüller, Efficiency of ab-initio total energy calculations for metals and semiconductors using a plane-wave basis set, Comput. Mater. Sci. 6 (1996) 15–50.
[45] G. Kresse, J. Furthmüller, Efficient iterative schemes for ab initio total-energy calculations using a plane-wave basis set, Phys. Rev. B. 54 (1996) 11169–11186.
[46] V. Wang, N. Xu, J.-C. Liu, G. Tang, W.-T. Geng, VASPKIT: A user-friendly interface facilitating high-throughput computing and analysis using VASP code, Comput. Phys. Commun. 267 (2021) 108033.
[47] J.P. Perdew, K. Burke, M. Ernzerhof, Generalized Gradient Approximation Made Simple, Phys. Rev. Lett. 77 (1996) 3865–3868.
[48] H.J. Monkhorst, J.D. Pack, Special points for Brillouin-zone integrations, Phys. Rev. B. 13 (1976) 5188–5192.
[49] J.D. Pack, H.J. Monkhorst, "Special points for Brillouin-zone integrations"---a reply, Phys. Rev. B. 16 (1977) 1748–1749.
[50] K.D. Myers, S.L. Bud'ko, V.P. Antropov, B.N. Harmon, P.C. Canfield, A.H. Lacerda, de Haas--van Alphen and Shubnikov--de Haas oscillations in $RAgSb_2$(R=Y,La-Nd,Sm), Phys. Rev. B. 60 (1999) 13371–13379.
[51] T. Arakane, T. Sato, S. Souma, T. Takahashi, Y. Watanabe, Y. Inada, Electronic structure of $LaAgSb_2$ and $CeAgSb_2$ studied by high-resolution angle-resolved photoemission spectroscopy, J. Magn. Magn. Mater. 310 (2007) 396–398.
[52] P. Ruszala, M.J. Winiarski, M. Samsel-Czekala, Dirac-Like Electronic-Band Dispersion of LaSb2 Superconductor and Its Counterpart $LaAgSb_2$, Acta Phys. Pol. A. 138 (2020).
[53] E. Lee, D.H. Kim, J.D. Denlinger, J. Kim, K. Kim, B.I. Min, B.H. Min, Y.S. Kwon, J.-S. Kang, Angle-resolved and resonant photoemission spectroscopy study of the Fermi surface reconstruction in the charge density wave systems $CeTe_2$ and $PrTe_2$, Phys. Rev. B. 91 (2015) 125137.
[54] D. Wu, Q.M. Liu, S.L. Chen, G.Y. Zhong, J. Su, L.Y. Shi, L. Tong, G. Xu, P. Gao, N.L. Wang, Layered semiconductor $EuTe_4$ with charge density wave order in square tellurium sheets, Phys. Rev. Mater. 3 (2019) 024002.
[55] P. Zhang, P. Richard, T. Qian, Y.-M. Xu, X. Dai, H. Ding, A precise method for visualizing dispersive features in image plots, Rev. Sci. Instrum. 82 (2011) 043712.
[56] P.V. Medeiros, S. Stafström, J. Björk, Effects of extrinsic and intrinsic perturbations on the electronic structure of graphene: Retaining an effective primitive cell band structure by band unfolding, Phys. Rev. B. 89 (2014) 041407.
[57] D.G. Trabada, J.I. Mendieta-Moreno, D. Soler-Polo, F. Flores, J. Ortega, DFT molecular dynamics and free energy analysis of a charge density wave surface system, Appl. Surf. Sci. 479 (2019) 260–264.
[58] X. Shi, P. Richard, K. Wang, M. Liu, C.E. Matt, N. Xu, R.S. Dhaka, Z. Ristic, T. Qian, Y.-F. Yang, C. Petrovic, M. Shi, H. Ding, Observation of Dirac-like band dispersion in $LaAgSb_2$, Phys. Rev. B. 93 (2016) 081105.
[59] B. Dardel, M. Grioni, D. Malterre, P. Weibel, Y. Baer, F. Lévy, Temperature-dependent pseudogap and electron localization in 1T-TaS_2, Phys. Rev. B. 45 (1992) 1462–1465.

[60] J. Schäfer, E. Rotenberg, S.D. Kevan, P. Blaha, R. Claessen, R.E. Thorne, High-Temperature Symmetry Breaking in the Electronic Band Structure of the Quasi-One-Dimensional Solid $NbSe_3$, Phys. Rev. Lett. 87 (2001) 196403.
[61] K. Rossnagel, On the origin of charge-density waves in select layered transition-metal dichalcogenides, J. Phys. Condens. Matter. 23 (2011) 213001.